ISSN: 0067-2904

Formation Evaluation and Petrophysical Analysis of Well Logging Data: an Example From Matruh-Shushan Basin, North Western Desert, Egypt

Amr M. Eid *, Walid M. Mabrouk, Ahmed Metwally
Geophysics Department, Faculty of Science, Cairo University, Giza, Egypt

Received: 21/3/2023 Accepted: 7/7/2023 Published: 30/8/2024

Abstract

Petrophysical evaluation of well logging data is crucial for exploring and improving oil and gas reservoirs. This involves obtaining reliable information about the rocks and fluids in the reservoir to estimate reserves and make informed decisions about drilling, production, and development strategies. In this study, data from six wells in the Matruh-Shushan Basin were evaluated using Log Quality Control procedures. Two zones of interest, Lower and Upper Safa members, were identified, and quantitative interpretation was conducted to determine the most effective parameters defining reservoir quality: Shale Volume, Effective Porosity, and Water Saturation. Results were positive, with promising net pay for both reservoirs. Numerical models and statistical methods were used to account for data uncertainties and provide reliable estimates of reservoir properties. The study highlights the significance of correct interpretation in successfully exploring and producing hydrocarbons.

Keywords: Matruh-Shushan Basin, Petrophysical Evaluation, Lower and Upper Safa, Quantitative Interpretation, North Western Desert.

1. Introduction

Formation evaluation and petrophysical analysis of well logging data are important in petroleum studies, as they provide valuable data used to assess the viability and productivity of oil and gas reservoirs. Well-logging tools measure various properties of subsurface rocks, such as porosity, permeability, lithology, fluid saturation, and formation pressure, which are essential in determining the potential productivity of a reservoir and making crucial decisions about drilling and production operations. These tools also enable monitoring well performance during production and identifying any changes in reservoir properties that could impact productivity. The petrophysical study was conducted using the Techlog software and offset well parameters. Techlog software, a product of Schlumberger, enables geoscientists and petroleum engineers to integrate and interpret various data types to identify reservoir fluids, such as oil and gas, and determine their distribution within the reservoir. By analysing well-log data, Techlog can help geoscientists and petrophysicists to estimate the reservoir's potential productivity, identify potential drilling targets, and optimise production operations. Surfer software also was used to produce contour maps that show the horizontal distribution of petrophysical parameters calculated from logs.

The purpose of our study is to provide an outlined petrophysical evaluation of Jurassic Upper and Lower Safa Members (Khatatba Formation) in the proximity of Matruh-Shushan

* Email : aeid@sci.cu.edu.eg

Basin in Egypt's Western Desert, shown in Figure 1a. This will help to better understand the reservoir and define the best development methods to improve the field's gas and condensate production. The Jurassic deposits are significantly developed in the Western Desert, which is located farther north. Shales, siltstones, and sandstones account for the majority of the continental facies [1]. Wadi El Natrun, Khatatba, and Masajid formation signify marine facies [2]. Six wells from the Matruh-Shushan Basin with the labels (AD-1, FA-1, GR-1, KA-1, OP-2, OP-1) are the target of this review; Figure 1b shows their locations.

2. Geological Settings

The Western Desert comprises the area west of the Nile River and encompasses over 700,000 km^2 or two-thirds of the total area of Egypt. In the southernmost region of the Western Desert pre-Paleozoic basement is exposed, which shows a regional slope towards the north direction, with an equivalent increase in the thickness of the sedimentary overlay, comprised entirely of Paleozoic, Mesozoic, also Tertiary to recent time formations [3]. Since 1990, numerous studies on the Western Desert's oil reserves suggested that about 90% of oil also 80% of the gas reserves have not yet been found [4].

Over 50% of Egypt's daily oil output comes from the Mesozoic age rift basins in the Northwestern Desert, including Shushan, Matruh and Alamein. These basins contain around 40% of Egypt's proven oil reserves [5]. Matruh-Shushan Basin which is generally recognised by thickening of sedimentary section towards North which is underlained by wide basement relief because of normal block faulting with minor compressional folding [6].

Age ranges in the northern Western Desert's sedimentary section extend from Early Paleozoic to Recent. The Carboniferous, Late Jurassic, Middle and Late Cretaceous, and Middle Miocene are four major sedimentary cycles that have been identified. Maximum southward transgression was a distinctive feature of these cycles. Maximum regressive episodes northward occurred throughout the Triassic and Early Jurassic, and they remained active across the Early Cretaceous and Late Eocene [7].

The sedimentary sequence of the Western Desert is made up of a series of tectonically and eustatically regulated depositional cycles as follows [8]:

- The oldest sedimentary rocks consist of sandstone, siltstone and shale and are characterised by a clastic facies cycle that covers the whole Paleozoic and Lower Jurassic formations.
- A carbonate section of middle and Upper Jurassic formations.
- The Lower Cretaceous and Upper Cretaceous make together a cycle of clastics (Early Cenomanian).
- Carbonate deposits in the northern Western Desert are again categorised as Upper Cenomanian and Upper to Middle Eocene.
- The Upper Eocene-Oligocene, Miocene, and newer sections form the uppermost clastic cycle.

The Khatatba Formation, a thick series of carbonaceous shale interbedded with porous sandstone, coal deposits, and limestone stripes, is a component of the Western Desert's overall stratigraphic column. Generalised stratigraphic column of the North Western Desert with highlight to Khatatba Fm, including Upper and Lower Safa members shown in Figure 2. The Matruh-Shushan Basin is the place of residence of the Middle Jurassic Khatatba Formation, which ranges in thickness from 283 to 358 m. Because of its ideal position concerning the source rock, Egypt's northern Western Desert is a desirable location for petroleum exploration. The Khatatba Formation's organic-rich rocks are believed to be the most productive source of oil and gas for accumulating within the Khatatba sandstone reservoir rocks.

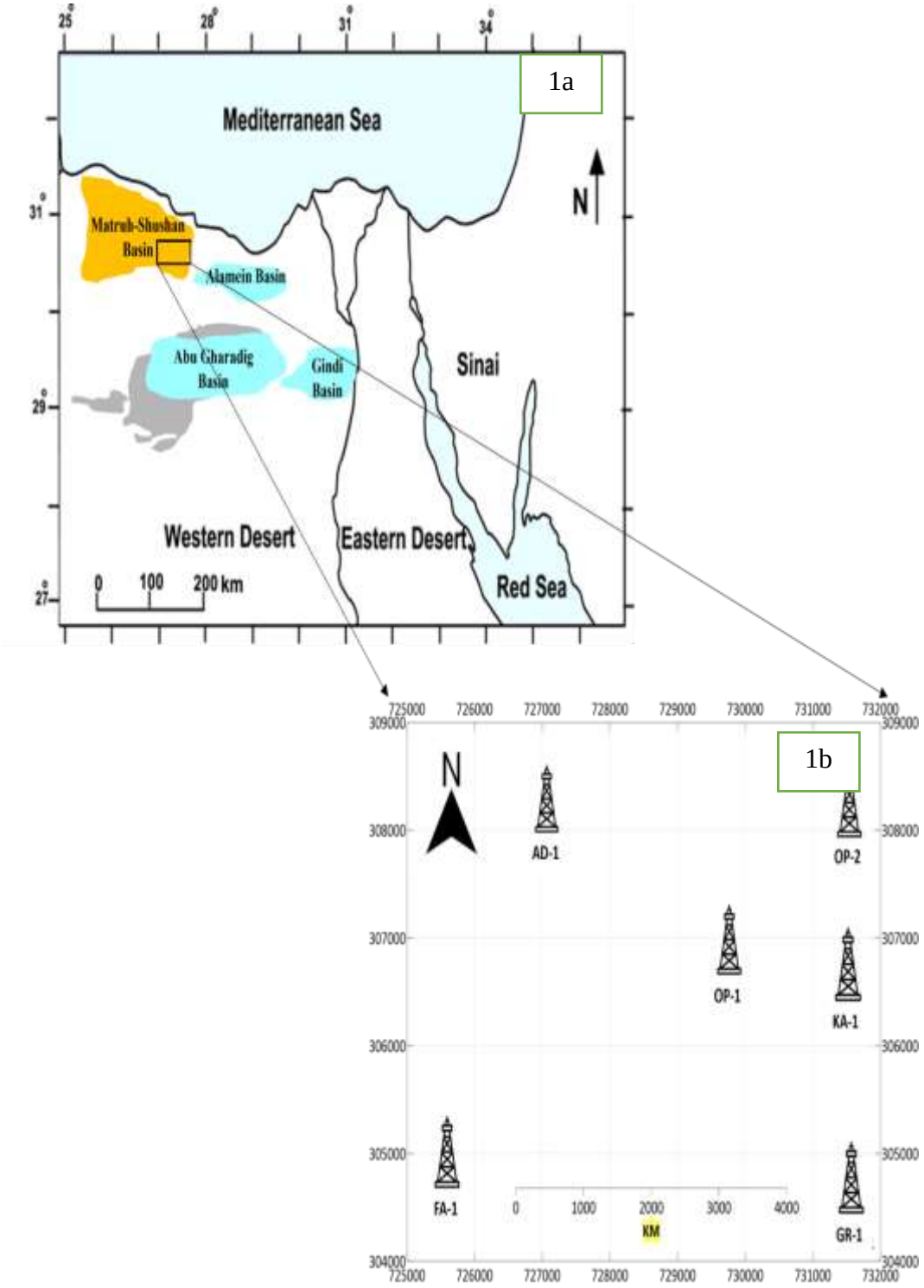

Figure 1: 1a Basins distribution in the northern Western Desert, Egypt (Modified after [30])

1b: Locations of the six wells in the study area.

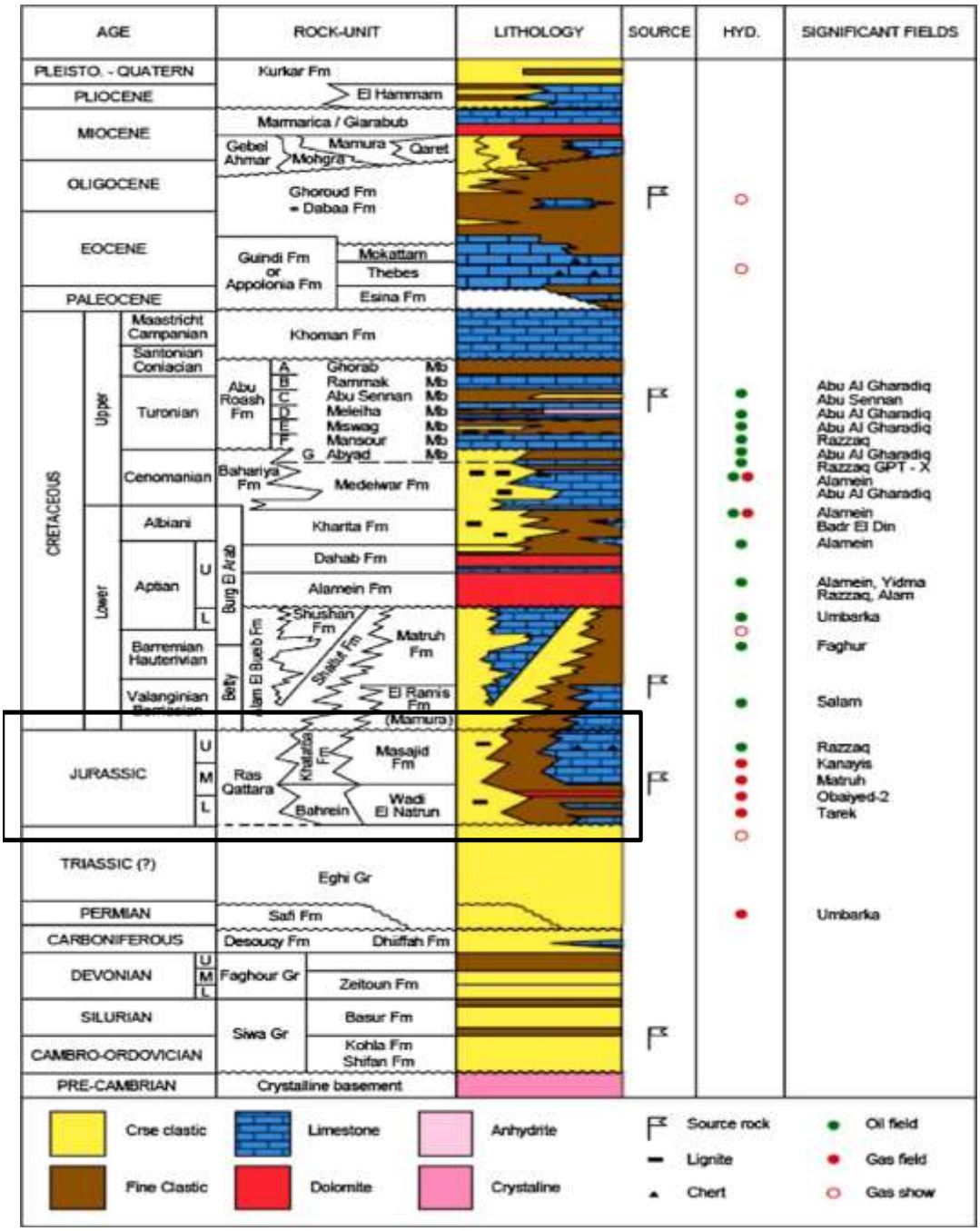

Figureure 2: Generalized stratigraphic column of the North Western Desert with highlight to Khatatba Fm including Upper and Lower Safa member; (Modified after [7]- [8]).

3. Data and Methodology

There are six wells in the research area with varying conventional log readings. Different log data readings consist of a Gamma-ray (GR) log, resistivity (MSFL, LLS, and LLD) logs and Neutron porosity (φN) log, Density (ρb) log with the formation tops delineated during drilling. A detailed Petrophysical Evaluation of the Jurassic Upper and Lower Safa Members (Khatatba Formation) was done on the available data using Techlog, 2015 and Surfer, 2019

did the Area Mapping. Figure 3 shows the petrophysical analysis that were performed on our case study and available data.

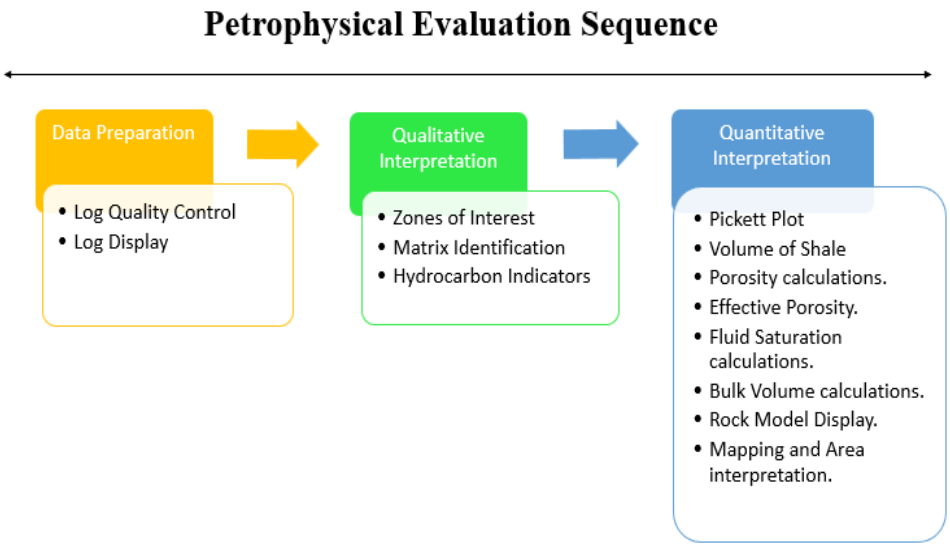

Figure 3:. Petrophysical Evaluation Sequence.

4. Petrophysical Evaluation

4.1. Data Preparation

4.1.1. Log Quality Control (L.Q.C)

We will start by applying the Log Quality Control Procedures because operating and service businesses have understood the issue of log quality management from the beginning of well logging. This issue worsens when the well logs are utilised for formation assessment[9]. If well logs are to be prepared successfully for evaluating formations, it is vital to get technically accurate well logs along with all the information that goes with them. Table.1 shows the LQC Procedures that must be done before starting interpretation.
The following factors should be thoroughly examined: -

Table 1: Log Quality Control Procedures.

Tool calibrations:	Calibrations of tools should be thoroughly evaluated prior to and after each job, and all recorded tools must be within the established tolerance range.
Depth control:	By comparing the log's Gamma-ray response with that of the previous run, the control of depth should be maintained verified for each run and each log.
Tension:	The tension curves should be closely monitored to determine when the tool became stuck.
Re-scaling:	This became essential to remove any spikes and rescale the recorded data using the typical standard scales across each log.
Selection of Model:	Based on the identified rock types, a suitable model is chosen, taking into consideration whether it is composed of sand, sand with shale, or has a more intricate rock structure.
Wash out & mud cake:	The well bore conditions could be assessed from borehole measurement log and drill bit diameter, determining the presence of washouts or a build-up of mud.

Shale-Parameter:	An essential step is to determine the characteristics of the shale (Density, porosity, sonic transit time, gamma ray, and resistivity), which can conveniently be obtained when drilling through a substantial shale layer.

4.1.2. Log Display

Figure 4 illustrates the well-logs data displayed after applying LQC for well (AD-1), which will be repeated for all the remaining five wells.

4.2. Qualitative Interpretation

4.2.1. Zones of Interest

In this section, a quickly review for our data was made, and then zones were selected that meet specific requirements. The most significant factor is a high increase in deep resistivity, with/without a gap between resistivity readings shallow/deep. The gap shows that the zone is washed away and that this formation primarily comprises hydrocarbon. Assessment for our zone reflects a lower gamma-ray response and an overlapping display of φN & ρb logs. Figure 5 shows the potential zone of interest with a low volume of shale, high effective porosity and hydrocarbon saturation.

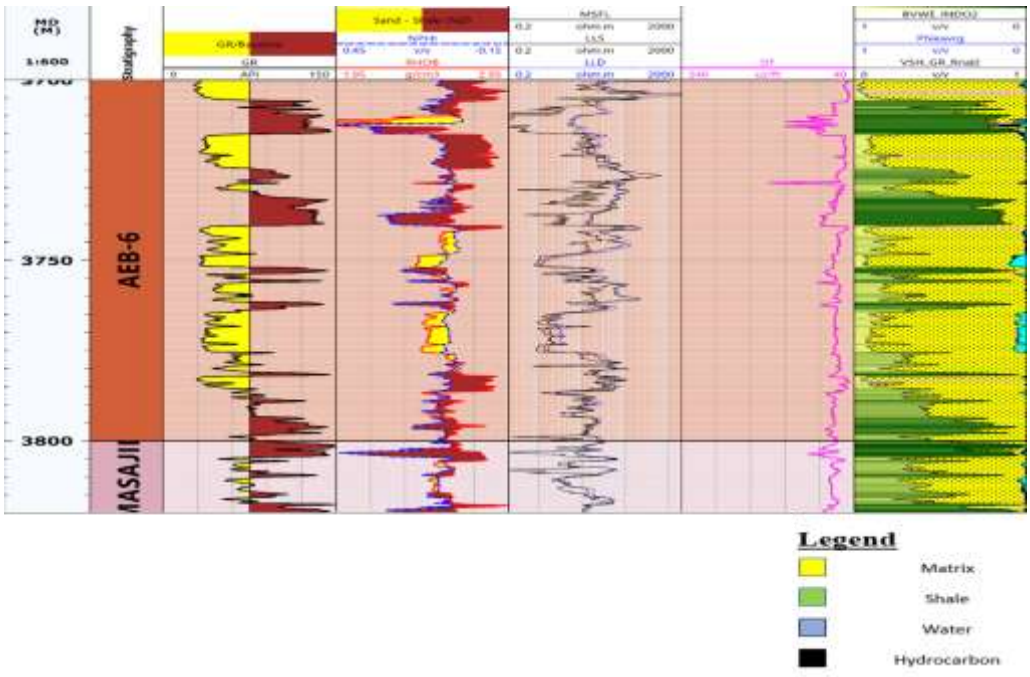

Figure 4:. Full Log Display after applying LQC.

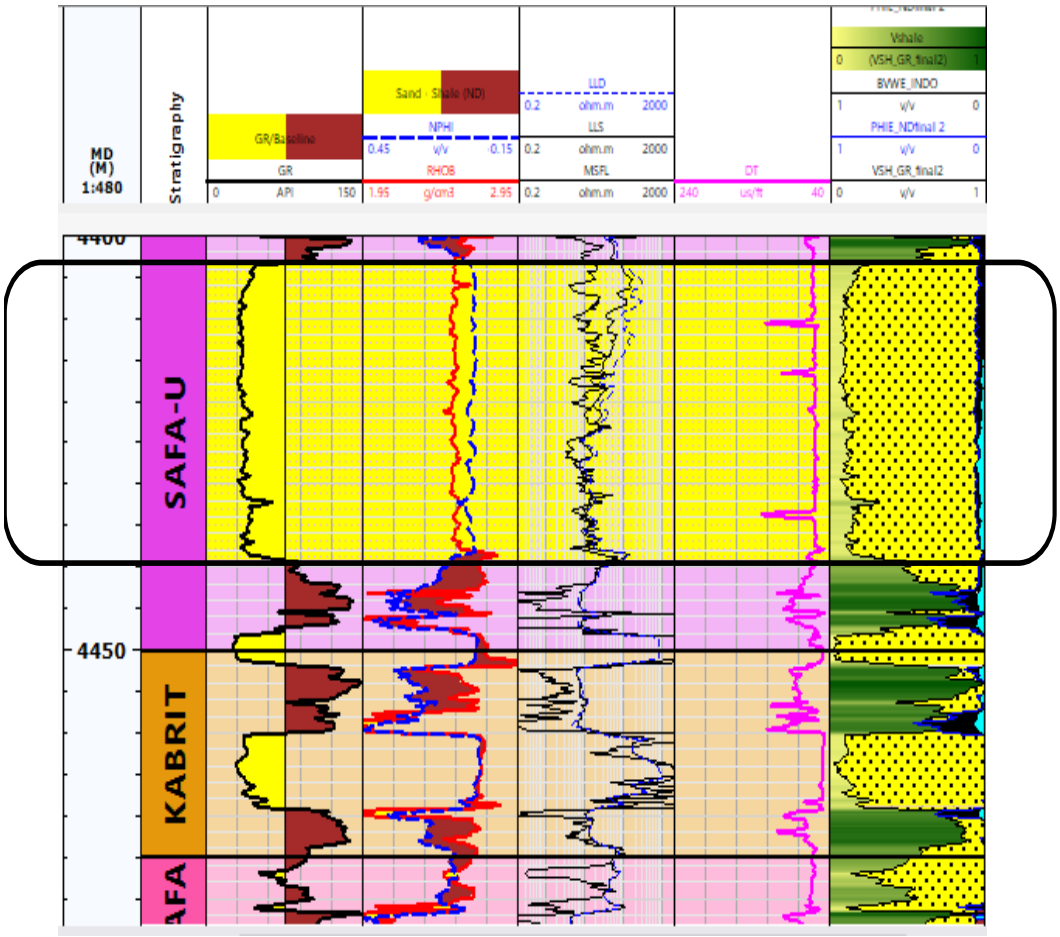

Figure 5: Highlighted Potential Zone of Interest.

4.2.2. Matrix Identification

For our study, we will use two techniques to verify the type of rock composition in our reservoir. The first is the M-N Plot, and the second is the MID Plot.

M-N diagram

In which the M value was obtained from the Density-Sonic cross-plot and the N value was obtained from the Neutron-Density cross-plot by the application of the two equations clarified below. Figure 6. M-N Cross-plot is displayed.

$$M = \frac{\Delta T_f - \Delta T_{log}}{\rho_b - \rho_f} * 0.01 \quad (1); \qquad N = \frac{\emptyset_{Nf} - \emptyset_{N-log}}{\rho_b - \rho_f} \quad (2)$$

Where:

ΔT_f Transit fluid time in the interval (185 for saltwater-based mud and 189 for freshwater-based mud).

ΔT_{log} Transit time of the formation in the interval.

ρ_f Density of fluid (1.1 for saltwater-based mud and 1 for freshwater-based mud).

ρ_b Formation bulk density.

$\emptyset_{Nf}$ Neutron porosity for fluid (approximately = 1).

$\emptyset_{N-log}$ Neutron porosity of the formation.

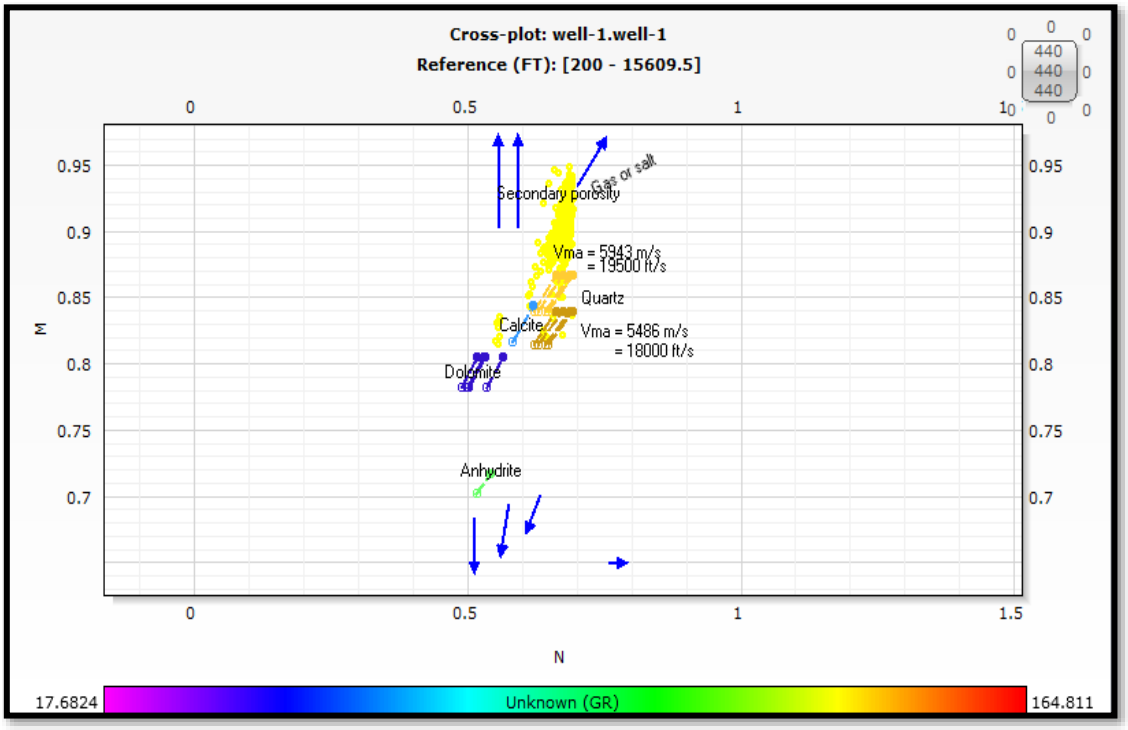

Figure 6: M-N Cross-plot.

MID plot

Using the MID plot, the apparent values of the (ρ_{ma}, g/cm3) vs the apparent sound transmission time (ΔT_{ma} ,sec/ft) are plotted against each other. The Density, neutron, and sonic curves are used to obtain the (ΔT,sec/ft), (ρ_b, g/cm3) and $\emptyset_N$ to determine these two parameters. From RHOB and NPHI cross plot shown in Figure 7, the Density of the matrix (ρ_{ma}, g/cm3) was obtained. and Figure 8, used to obtain the apparent sound transmission time of the matrix (ΔT_{ma} , sec/ft). Figure 9. MID chart is displayed.

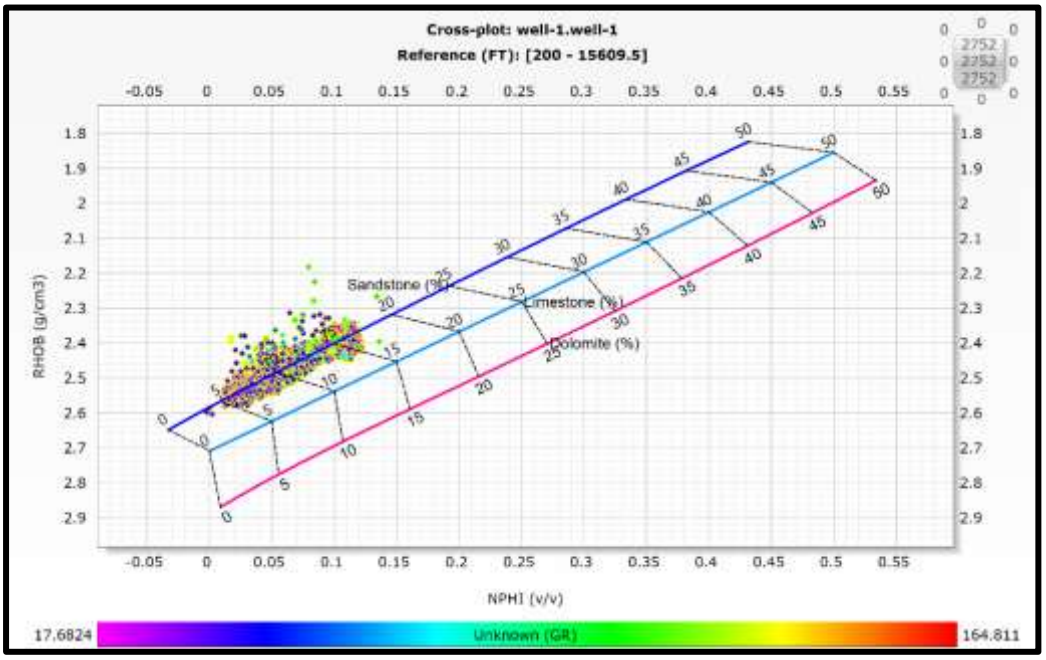

Figure 7:. RHOB and NPHI cross plot.

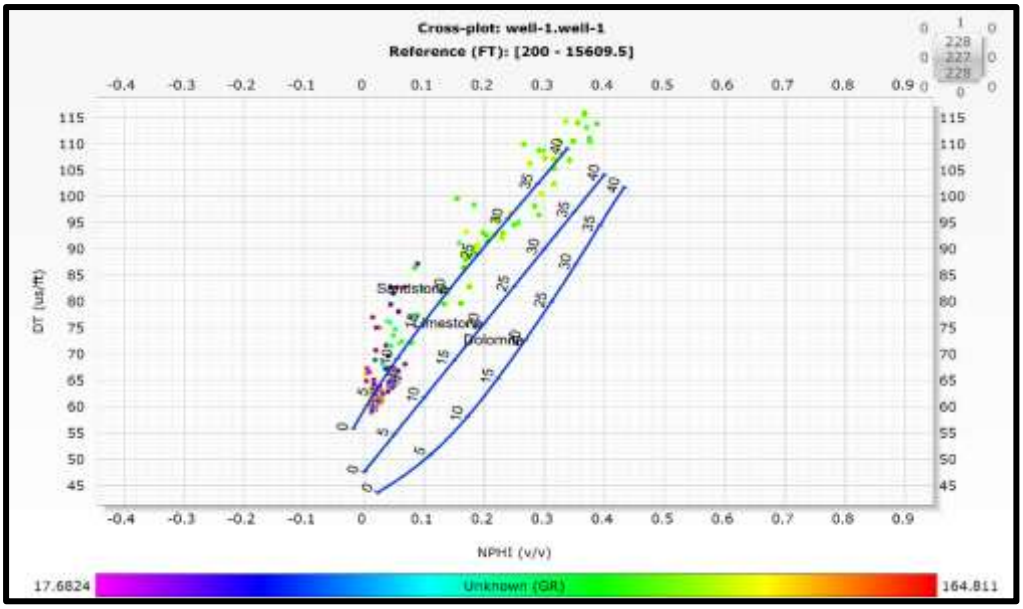

Figure 8: DT and NPHI cross plot.

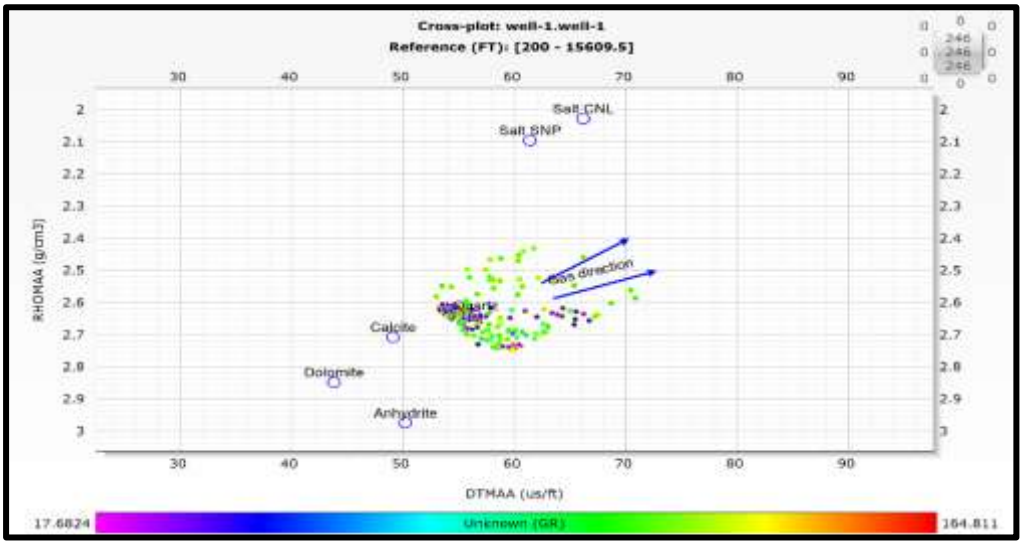

Figure 9: MID chart.

4.2.3. Hydrocarbon Indicators

It is noteworthy to specify which sections require a thorough evaluation of the formation, as only those containing hydrocarbon require on-site examination. With the need to quickly assess thousands of feet of borehole, techniques were developed to eliminate "wet" intervals and promptly identify potential "oil-rich" intervals. The five most commonly used hydrocarbon indicators [10, 11, 12, 13] are as follows:

1. Apparent water resistivity (Rw).
2. FR–Ro overlays. [14]
3. Movable oil plot (MOP).
4. The Rxo/Rt indicator.
5. The neutron–density overlay.
6. Bulk Volume of Water (BVW). [15]

In the present study, only three techniques would be used, which are: (a) FR–Ro overlays, (b) Movable oil plot (MOP), (c) neutron–density separation.

FR–Ro overlays

FR-Ro overlays technique, introduced by [16], involves the use of the following equation of water saturation:

$$S_w = \frac{FR.R_w}{R_t} \quad (3)$$

Rewrite equation (3), gives:

$$R_t.S_w = FR.R_w \quad (4)$$

$$FR = \frac{R_o}{R_w} \quad (5)$$

where S_w is the saturation of water in the non-invaded zone and expressed as a fraction or percentage, n is the saturation coefficient (generally put as 2), R_w is the resistivity of water in formation (its unit is ohm-meter), R_t is the formation actual resistivity (its unit is ohm-meter), and FR is the formation factor (unitless).

In water-bearing zones, where $S_w = 100\%$, Eq. (4) can be represented by Eq. (5). By plotting R_o and FR against depth, we can easily distinguish between water-bearing and hydrocarbon-bearing zones, given the knowledge of R_w, where:

1. In areas containing water, R_o is nearly identical to FR (Figure 10).
2. In zones containing hydrocarbons, there is a noticeable gap between R_o and FR (Figure 11).

Movable oil plot (MOP)

When both the invaded and uninvaded zones of the formation are entirely saturated with water (S_{xo} and S_w=100 %), the formation factor is defined as:

$$F = \frac{R_t}{R_w} \; ; \; F = \frac{R_{xo}}{R_{mf}} \quad (6)$$

Nevertheless, if the formation is not entirely submerged in water ($S_w < 100\%$) , which means there is a hydrocarbon, then:

$$\frac{F}{S_w^n} = \frac{R_t}{R_w} \; , \; F < \frac{R_t}{R_w} \quad (7)$$

$$\frac{F}{S_w^n} = \frac{R_{xo}}{R_{mf}} \; , \; F < \frac{R_{xo}}{R_{mf}} \quad (8)$$

- The separation between F and $\frac{R_{xo}}{R_{mf}}$ curves will reveal whether residual hydrocarbon is present.
- $\frac{R_{xo}}{R_{mf}}$and $\frac{R_t}{R_w}$ curve separation, however, the existence of movable hydrocarbons will be visible.
- Figure 12 shows the Plot of Movable Oil.

The neutron–density separation

When they're plotted on equivalent scales, neutron-density response (Figure 13) could be used as an indicator of hydrocarbon.

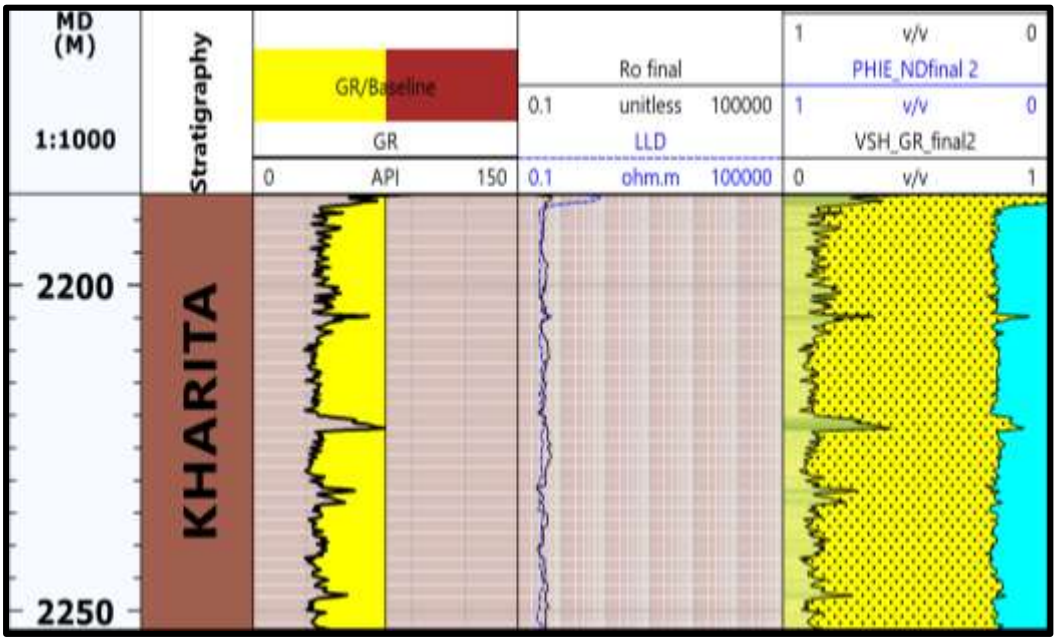

Figure 10: FR-Ro Overlay (Water Bearing Zone).

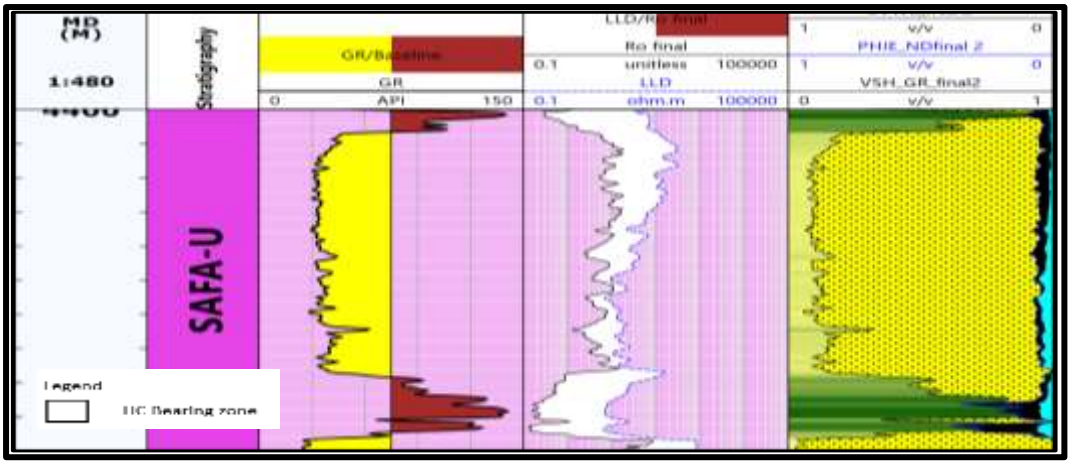

Figure 11: FR-Ro Overlay (HC Bearing Zone).

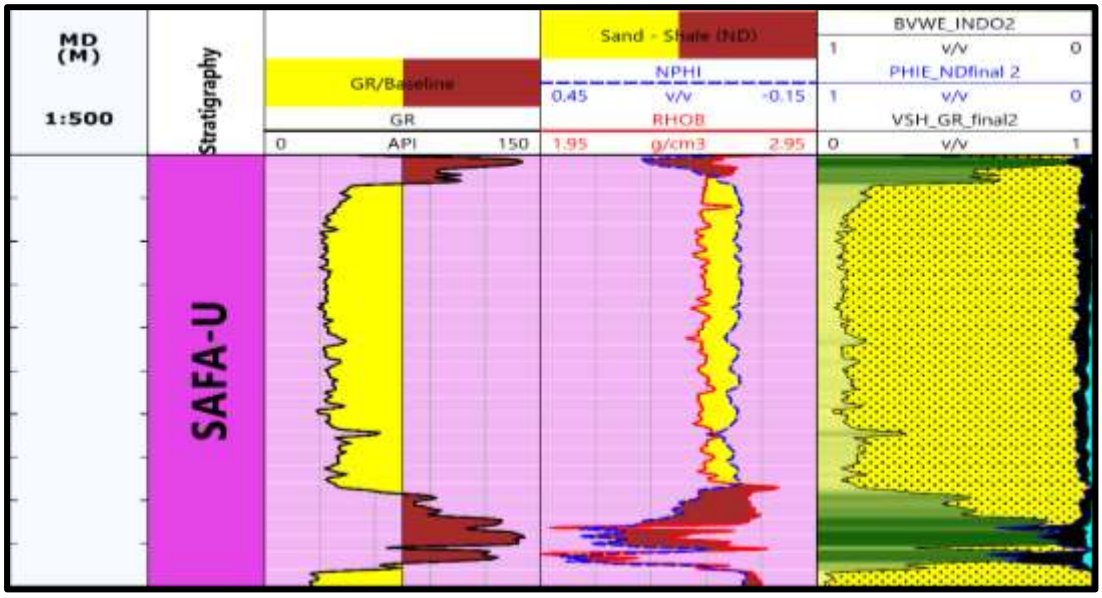

Figure 12: Movable Oil Plot (MOP).

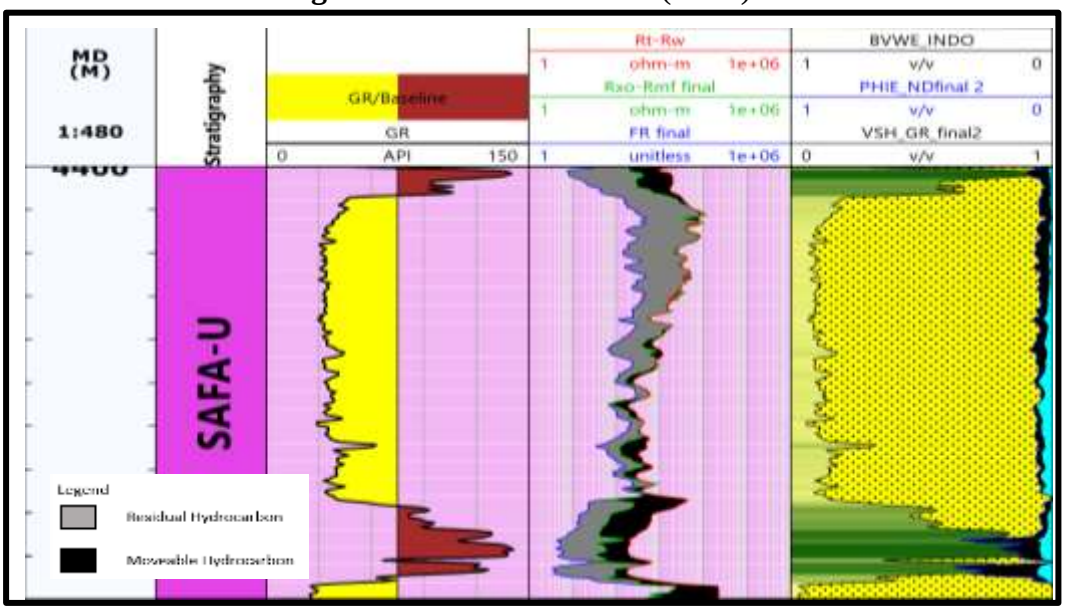

Figure13: Neutron–Density overlay.

4.3. Quantitative Interpretation

4.3.1. Pickett plot and Rw calculations

The plot is a two logarithmic representation of resistivity value on x-axis and porosity measurement on y-axis [17]. This plot is based on taking the Archie equation's logarithm [16].

Equation of Archie for formation resistivity factor (F), porosity ($\emptyset_N$), water saturation (S_w), and resistivity of water (R_w) in particulate rocks implies that:

$$F = R_o R_w = \frac{a}{\emptyset^m}, \quad (9)$$

$$S_w^n = R_o R_t, \quad (10)$$

In which:

a, proportionality factor (in range of 0.5 to 1.4);

m, cementation component (in rang of 1.25 to 2.95);

n, The saturation coefficient, which is commonly put as 2;

R_o, formation's resistivity at 100 percent water saturation;

R_w, The resistivity of water in formation.;

R_t, The accurate true formation resistivity;

Hence, from two Eqs. (9) and (10), we have:

$$m\ log\ (\emptyset) = log\ aR_w - log\ R_t - n\ log\ S_w, \quad (11)$$

The cementation factor can be calculated by plotting lines of constant water saturation (S_w), which will create a straight line with a negative slope (m). After water line is constructed, additional parallel lines to various (S_w) values can be drawn under the assumption of a constant n. (usually 2). By determining Ro, then Rw can be calculated. Figure 14. Pickett Plot.

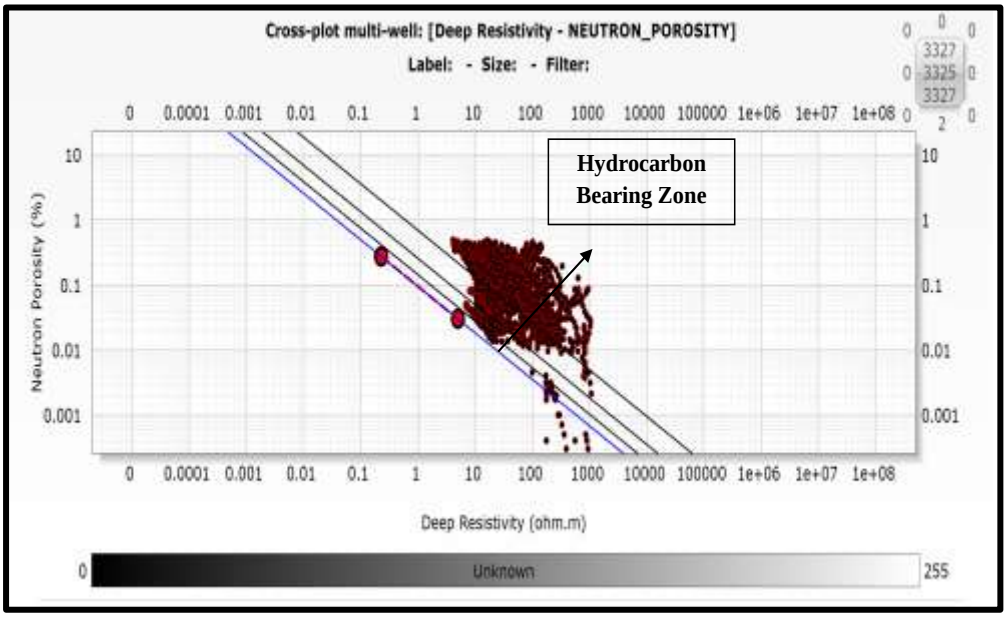

Figure14: Pickett Plot.

4.3.2. Volume of Shale calculations

Among petrophysical qualities, Vsh is the most essential as well as basic reservoir characteristic that determines how much shale is contained in hydrocarbon reservoirs [18]. It plays a crucial role in the precise estimation of other petrophysical characteristics like effective porosity, water saturation, permeability and Net to Gross, all of which are crucial for figuring out reservoir quality, hydrocarbon potential, and the realistic estimation of hydrocarbon reserves. Numerous techniques for determining a reservoir's Vsh from well logs have been thoroughly studied in the literature. Obtaining a trustworthy evaluation for shale is executed via utilising as many markers as feasible. Comprehensive overviews of the analysis of shale formations have been presented in excellent reviews by [12, 19].

In our study, the following steps will be taken to determine the volume of shale:

First, we will compute the shale volume from linear gamma-ray index equation. Next, we will adjust the calculated shale volume using the method proposed by [20]. In the end, we will categorise the formation based on the shale content as clean, shaly, or shale, and distinguish between effective and ineffective shale.

Linear gamma-ray index equation:

$$I_{GR} = \frac{GR_{log} - GR_{min}}{GR_{max} - GR_{min}} , \quad (12)$$

Steiber equation (1973) to adjust the calculated shale volume:

$$V_{sh} = \frac{0.5 * I_{GR}}{1.5 - I_{GR}} , \quad (13)$$

In which:

I_{GR} $gamma\ ray\ index$;
Vsh $volume\ of\ shale$;
$GRLog$ $gamma\ ray\ reading$;
$GRmax$ $maximum\ gamma\ ray\ (shale)$;
$GRmax$ $minimum\ gamma\ ray\ (clean\ sand\ or\ carbonate)$.

4.3.3. Porosity calculations

According to [21], porosity known as the percentage of vacuum space that is present in a given volume, with values ranging from 0% (no voids) to 100% (completely solid). However, porosity values for porous medium examined in applications for reservoir assessment typically range from 0 to about 30%. Rocks with pores may contain gas, oil, or water phases in actual reservoir conditions (or a mixture). Only the linked rock pores between these phases can be efficiently retrieved. Effective porosity is the measure of pore vacuum inside a medium that contributes to permeability and permits flow through it [22]. The ratio of void space within a medium shows a certain kind of connection over its whole volume. Because it estimates the whole volume from which extraction is conceivable if filled with hydrocarbons, effective porosity is considerably more crucial than actual porosity for petrophysicists.

To estimate the effective porosity from logs, we will use some equations described in detail below in which we will calculate the Total Porosity from $\emptyset_N$ log and from ρ_b log, which is called $\emptyset_D$ as follows:

$$\emptyset_D = \frac{\rho_m - \rho_b}{\rho_m - \rho_{fl}}, \quad (14)$$

$$\emptyset_T = \frac{\emptyset_N + \emptyset_D}{2}, \quad (15)$$

$$\emptyset_{eff} = \emptyset_T - (V_{sh} * \emptyset_{sh}), \quad (16)$$

Where:

$\emptyset_D$ $Porosity\ from\ density\ log;$
ρ_m $Density\ of\ matrix;$
ρ_b $Density\ from\ log;$
ρ_{fl} $Density\ of\ Pore\ fluids;$
$\emptyset_T$ $Total\ Porosity;$
$\emptyset_{eff}$ $Effective\ Porosity;$
V_{sh} $Volume\ of\ shale;$
$\emptyset_{sh}$ $Porosity\ of\ shale;$

4.3.4. Fluid Saturations calculations

Typically, reservoir rocks contain both hydrocarbon and water (commonly referred to as connate or interstitial water). Saturation represents the percentage of pore volume filled with a specific fluid (such as water, oil and gas) and can be put into mathematical form:

$$Fluid\ Saturation = \frac{Total\ voulme\ of\ the\ fluid}{Pore\ volume}$$

All saturations are calculated based on the pore volume, not the overall volume of the reservoir. Each fluid's saturation ranges from 0 to 100%, and the sum of all saturations equals 100%. The saturation of connate water (Swc) is significant because it considers the space between oil and gas and is not uniformly distributed across the reservoir, varying based on factors such as rock type, permeability, and height relative to the free water table.

Clean Formations

There are several methods for determining the water saturation in formations with uniform intergranular porosity and no shale content. The first and most popular water saturation equation, according to [16], is:

$$S_w^n = \frac{F_R R_w}{R_t} \quad (17)$$

where S_w is the saturation of water in the non-invaded zone and expressed as a fraction or percentage, n is the saturation coefficient (generally put as 2), R_w is the resistivity of water in formation (its unit is ohm-meter), R_t is the formation actual resistivity (its unit is ohm-meter), and F_R is the formation factor (unitless).

Flushed zone Water Saturation (S_{xo}) has a similar equation.

$$S_{xo}^{n} = \frac{F_R R_{mf}}{R_{xo}} \quad (18)$$

where S_{xo} is a saturation of water in the flushed zone (percentage/ratio), n is the saturation coefficient (put as 2), R_{mf} is resistivity mud filtrate (unit is ohm-meter), R_{xo} is the flushed zone resistivity (unit is ohm-meter), and F_R is the formation factor (unitless).

Another way for calculating water content in clean formation is the R_{wa} method [23]. In this aspect, the Archie water saturation changes if water saturation is considered to be 100%.

$$R_{wa} = \frac{R_t}{F_R} \ , \quad (19)$$

The R_{wa} symbol accounts for the apparent water resistivity, which is only equal to R_w in 100% water bearing formations. As a result, the R_{wa}, the approach can be effective for locating prospective hydrocarbon-bearing zones and for calculating R_w values. In practice, R_{wa} is calculated by simply dividing F_R derived from a porosity log by deep resistivity (LLD). It is more efficient to either perform a continuous R_{wa} computation throughout a significant portion of borehole or to perform numerous laborious computations to approach a continuous estimation.

Shaly Formations

In log analysis, identifying shales or even shaly formations is critical. They have a significant impact on calculations of porosity, as we already discussed, but also on determining fluid saturation due to their electrical properties. For this case, [16]suggested an improved version of his equation that took the parameters of shale into account.

$$S_w = \sqrt{F R_w \times \left(\frac{1}{R_t} - \frac{V_{sh}}{R_{sh}}\right)} \ , \quad (20)$$

where S_w is the saturation of water in the non-invaded zone and expressed as a fraction or percentage, n is the saturation coefficient (generally put as 2), R_w is the resistivity of water in formation (its unit is ohm-meter), R_t is the formation actual resistivity (its unit is ohm-meter), and F_R is the formation factor (unitless), R_{sh} is shale resistivity (unit is ohm-meter), and V_{sh} is volume portion of shale.

[24]created a prototype that included clay spread across a clean sand structure. Alternatively, the distributed shale should produce an equation of the form of:

$$Ax^2 + Bx + C = 0 \ , \quad (21)$$

Then Water Saturation can be calculated using the new form as follows:

$$S_w = \frac{R_w}{2\emptyset}\left[-y + \sqrt{y^2 - \left(\frac{4}{R_w}\right) \times \left(\frac{V_{sh}^2}{R_c} - \frac{1}{R_t}\right)}\right], \quad (22)$$

His observations indicate that the water saturation values in low resistivity pay sands are too low, but these values turn positive in the case of possible shaly pay sand.

[25] proposed the complete shale equation in his detailed research, which was verified by lab experimentation at French Petroleum Institute. His equation is expressed as

$$S_w = \left[\left(\frac{-V_{sh}}{R_{sh}}\right) + \sqrt{\frac{-V_{sh}}{R_{sh}} + \frac{5\emptyset^2}{R_t R_w}}\right] * \frac{0.4 R_w}{\emptyset^2} \quad (23)$$

The entire shale model, which Schlumberger represented in 1969, has been realised to be effective among values range of water saturation experienced in actuality. The following equation gives the representation produced by this model.

$$S_w = \sqrt{\left(\frac{R_o}{R_t}\right) + \left(\frac{R_o V_{sh}}{2R_{tsh}}\right)^2} - \left(\frac{R_o V_{sh}}{2R_{tsh}}\right), \quad (24)$$

The Indonesian model was created by [26] the change in calculated water saturation represents it (S_w) as a function of true resistivity (Rt) and reservoir rock shale content.

$$S_w = \left[\frac{V_{sh}^{0.5(1-V_{sh})}}{\left(\frac{R_{sh}}{R_t}\right)^{0.5} + \left(\frac{R_{sh}}{R_0}\right)^{0.5}}\right]^{\frac{-2}{n}}, \quad (25)$$

Schlumberger, in 1972, on the contrary, introduced a modified total shale model at which the value (1−Vsh) is considered. The next equation defines the model:

$$S_w = \left(\frac{R_o V_{sh}}{2R_{tsh}}\right)(1 - V_{sh})\left(\sqrt{\left(\frac{R_t}{R_o}\right)(1 - V_{sh}) + \left(\frac{R_o V_{sh}}{2R_{tsh}}\right)^2 (1 - V_{sh})}\right), \quad (26)$$

A further involvement for calculating water saturation which performs better in various circumstances, was made by [27].

$$S_w = \frac{\left(\frac{-V_{sh}}{R_t}\right) + \sqrt{\left(\frac{-V_{sh}^2}{R_{tsh}^2}\right) + \frac{\emptyset_T^2}{0.2R_t R_w(1-V_{sh})}}}{\frac{\emptyset_T^2}{0.4R_t R_w(1-V_{sh})}}, \quad (27)$$

We employed the Indonesian model created by [26] for the current study. The bulk volume of water was calculated by multiplying the calculated water saturation (S_w) and its corresponding porosity (∅). In the final stage of quantitative interpretation, the bulk water volume will be employed, as well as the bulk rock model:

$$BVW = S_w \times \emptyset, \quad (28)$$

In which: $BVW\ is\ Bulk\ volume\ of\ water$;
$S_w\ is\ water\ saturation\ of\ uninvaded\ zone$;
$\emptyset\ is\ porosity$;

4.3.5. Bulk Volume calculations

The overall volume of fluid, which is shown in Figure 15, that needs to be calculated equal to the sum of all fluids exist in the effective porosity of the zone that the formation where have invaded:

$$\emptyset_T = BVW_{sh} + \emptyset_{eff}, \quad (29)$$

$$\emptyset_{eff} = BVW + BVHC, \quad (30)$$

$$BVW = BVW_m + BVW_{ir}, \quad (31)$$

$$BVHC = BVHC_m + BVHC_r, \quad (32)$$

where:

BVW_{sh} $bulk\ volume\ of\ water\ related\ to\ shale\ portion; which\ is\ water\ portion\ trapped\ in\ shale, wated\ bounded\ to\ shale\ surface\ and\ water\ absorbed\ by\ shale\ molecules$;
BVW $bulk\ volume\ of\ water$;
$BVHC$ $bulk\ volume\ of\ hydrocarbon$;
BVW_m $bulk\ volume\ of\ movable\ portion\ of\ water$;
BVW_{ir} $bulk\ volume\ of\ irreducible\ portion\ of\ water$;
$BVHC_m$ $bulk\ volume\ of\ movable\ portion\ of\ hydrocarbon$;
$BVHC_r$ $bulk\ volume\ of\ residual\ portion\ of\ hydrocarbon$;

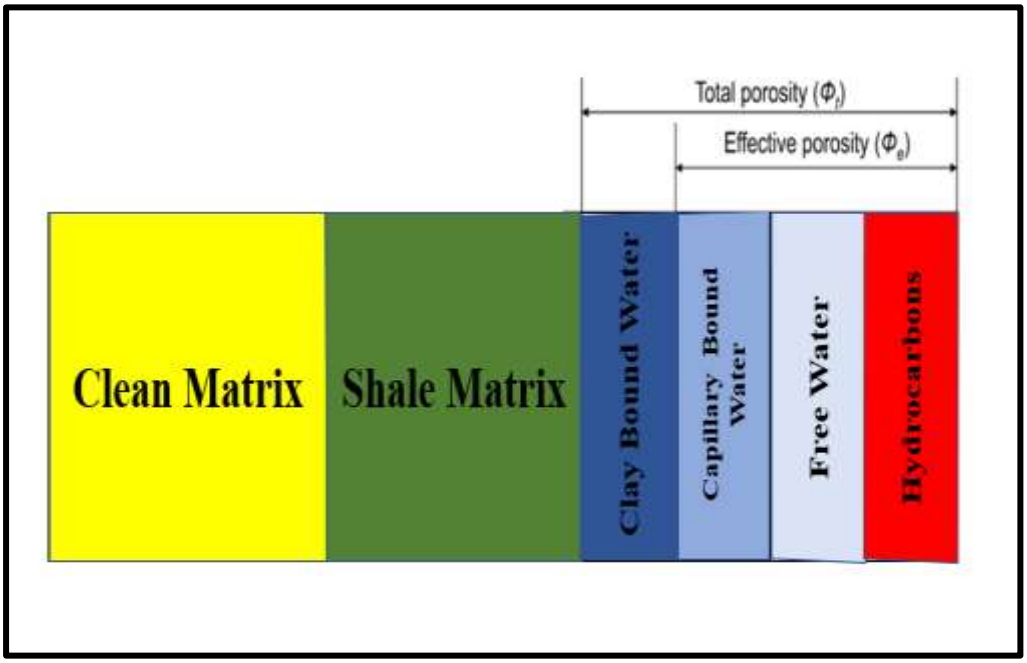

Figure 15: Bulk volume of rock.

4.3.6. Rock Model Display

It serves as a reliable petrophysical interpretation model [13]. It explains the formation division as depicted in Figure 16 and is presented as a log in Figure 17. Shale volume, effective porosity, and bulk water volume are the three computed petrophysical characteristics of the bulk rock volume. Our model will clear the matrix volume percentage, shale volume, and degree of hydrocarbon content saturation.

The volume of the matrix is broken down into parts, such as sandstone, limestone, dolomite etc. The bulk rock model can be written as an equation as follows:

$$1 = V_{sh} + V_{ma} + \emptyset_{eff}\,, \tag{33}$$

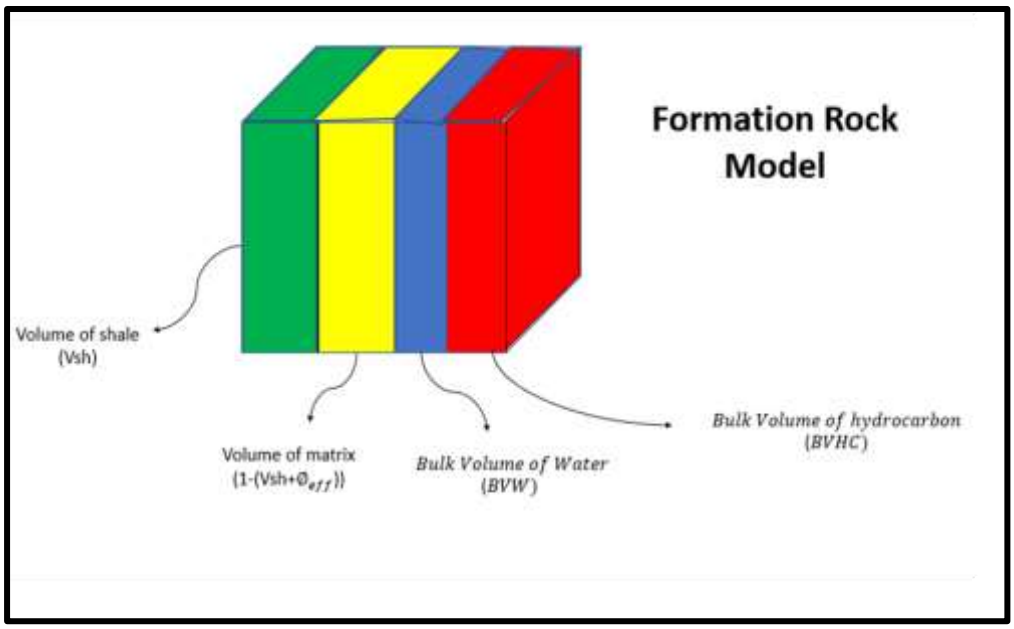

Figure 16:. Formation Rock Model.

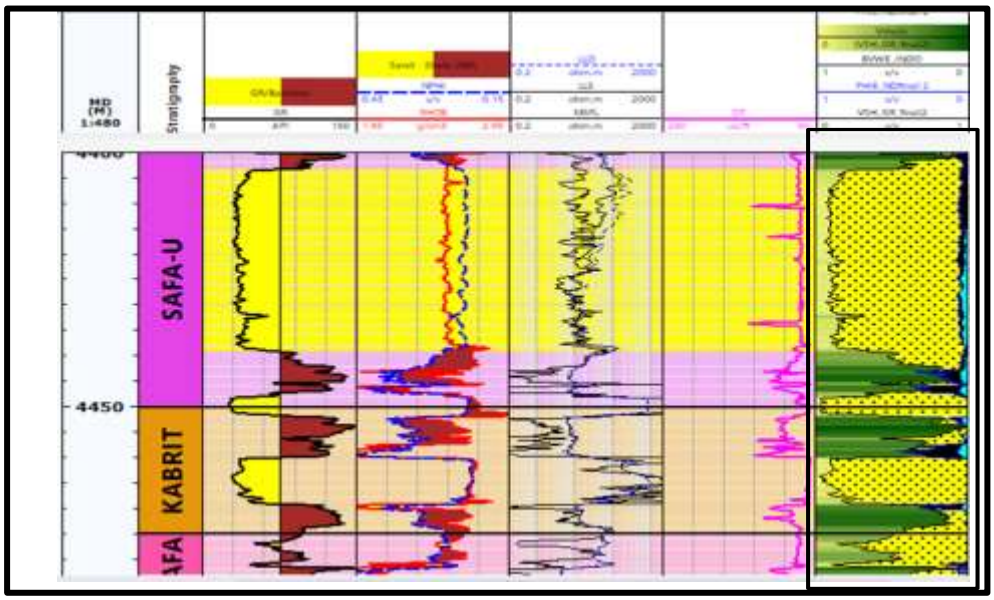

Figure 17: Highlighted portion is the Formation Rock Model of well AD-1.

4.3.7. Mapping and Area Interpretation

A total of six wells were used in this study. Maps are used to display the horizontal distribution of petrophysical parameters calculated from logs (effective porosity, water saturation and shale volume) [29]. Thus, we made contour mapping between the six wells for studying the distribution of (1) Volume of Shale, (2) Effective porosity and (3) Water Saturation. These maps allow us to better our area of interpretation and predict the best reservoir quality at which location. For our area and from the data available, we selected two formations of interest to map: Lower & Upper Safa.

From the contour maps, we found a decrease in the volume of shale towards NE (North-East) direction for the two formations and an increase in the effective porosity towards the same direction. For the water saturation, we marked an increase in the SE (South-East) direction and a decrease towards NE (North-East) direction for the two formations.

Finally, we have to say that the reservoir quality for Lower and Upper Safa formations increases towards the NE direction, at which we found a low volume of shale, high effective porosity and low water saturation. So, we highly recommend drilling new development wells towards the NE direction for the best reservoir quality.

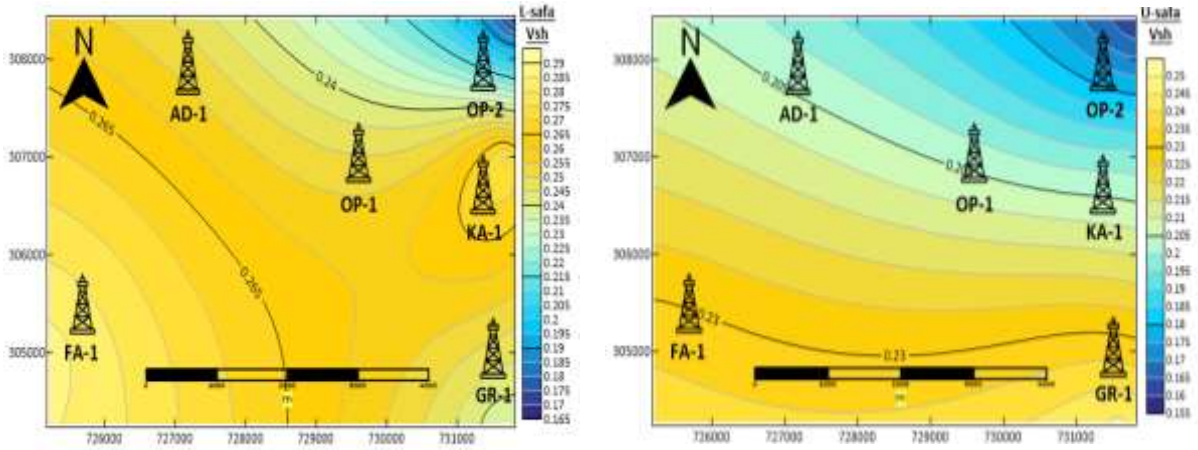

Figure 18: volume of shale contour maps for Lower and upper Safa Fm.

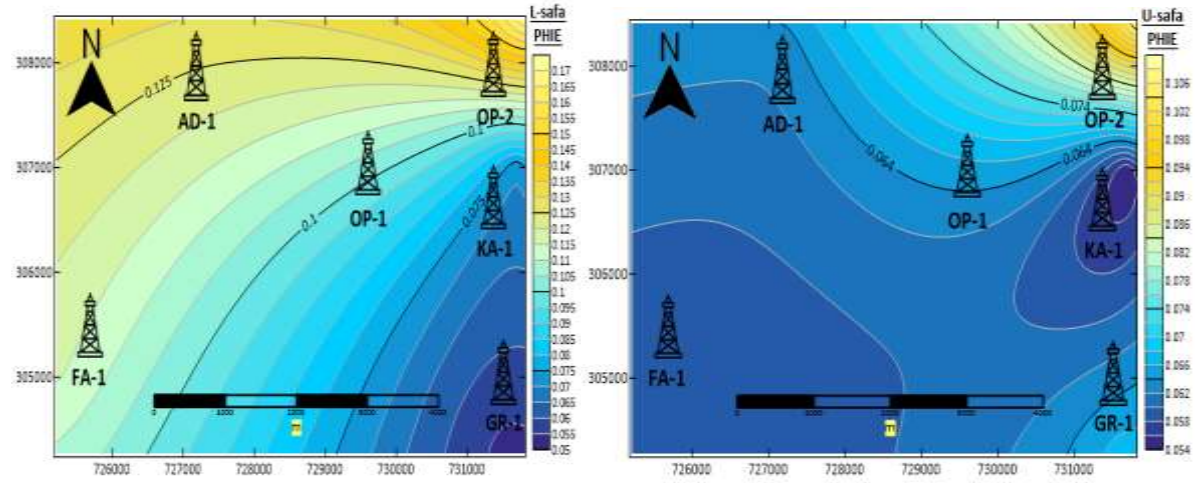

Figure 19: Effective Porosity contour maps for Lower and upper Safa Fm.

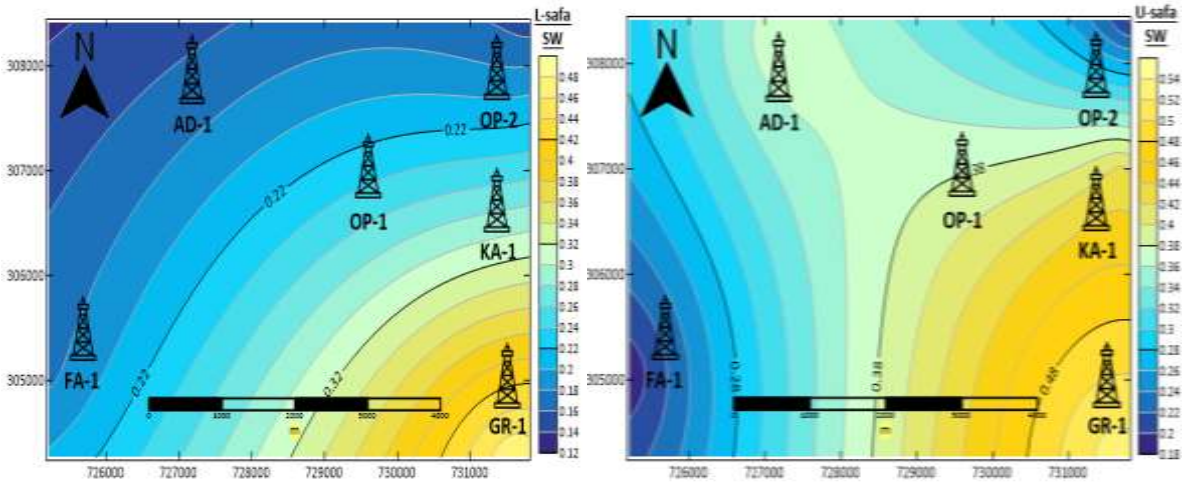

Figure 20: Water Saturation contour maps for Lower and upper Safa Fm.

5. Results and discussions

Through our study and computations, we followed the sequence of petrophysical evaluation mentioned in Figure 3. Started by applying quality controls on available logs (Table-1), which improved the quality of the data available to interpret them better. Then on certain criteria mentioned above, two zones of interest were chosen: Lower & Upper Safa. For these two zones, we found from M-N cross plot (Figure6) that the lithology is gas sand also, the MID plot (Figure9) confirms this lithology. Then, three methods of hydrocarbon indicators agreed with the previous plots that the two zones of interest contain hydrocarbon.

In quantitative interpretation, the computations give the proportionality factor (a = 1), cementation component (m = 1.4), the saturation coefficient (n = 2) and the resistivity of water in formation (Rw = 0.037) from Pickett plot (Figure14). Second, calculated the shale volume from linear gamma-ray index equation (Eq.12) and corrected shale volume using Steiber equation (Eq.13) from which we noticed that the two members of interest (Lower & Upper Safa) consists of sand and shale intercalations. Then, the values of effective porosity were extracted from (Eq.16). Finally, the water saturation was calculated from the Indonesian

model (Eq.25). Table.2 shows the output of the quantitative calculations. From (Eq.28), the Bulk volume of water was estimated, which is used along with the volume of shale and effective porosity to make the Formation Rock Model displayed in (Figure17).

The values represented in (Table-2) are used to construct contour maps to the area illustrated in (Figures 18 to 20). Our interpretations of these maps showed that the reservoir quality for the Lower and Upper Safa formations improves towards the northeast, where we discovered a limited amount of shale, high effective porosity, and low water saturation. As an outcome, we strongly advise drilling new development wells in the NE direction for optimum reservoir quality. The petrophysical analysis and quantitative interpretation showed that the U-Safa member is more promising than the L-Safa member in all wells except well-6, at which the two members are missing.

Schlumberger Techlog software was used to correlate the chosen logs from the wells. The correlation uses the standard measured depth as a depth metric. The results obtained can be seen in Figure21, which shows a well- correlation between Lower & Upper Safa Members.

From our correlation, well-3 appeared to be structurally lower than the remaining wells, suggesting that well-3 is drilled on a graben structure. Kabrit member, a member between Lower and Upper Safa, disappeared in well-4 due to pinch-out. The upper Safa member is relatively the same thickness across the wells, while thickening occurred to Lower Safa member in the east direction.

The correlated logs in the figure are the volume of shale, matrix portion, which is sand, water and hydrocarbon saturations in which the combination of those logs represents the litho-saturation model known as the formation rock model. From these correlated logs, the best reservoir quality parameters are found across well-5, which appeared to have the lowest volume of shale and a promising amount of hydrocarbon.

Finally, the area of study is very promising and could produce a commercial number of hydrocarbons based on our interpretation of the available data in which all the methods used during this research confirm each other and confidently say that these results are trustworthy.

Table 2: Petrophysical Evaluation for Lower and upper Safa Fm.

Well	Zones	Top	Bottom	Unit	Gross	Net	Vsh Fraction	PHIE Fraction	Sw Fraction
AD-1	SAFA-U	14025.59	14599.74	FT	574.146	222.5	0.199	0.063	0.377
AD-1	SAFA-L	14681.76	15609.5	FT	927.741	95.25	0.25	0.128	0.157
FA-1	SAFA-U	14189.63	14763.78	FT	574.146	263.3	0.234	0.059	0.185
FA-1	SAFA-L	14845.8	15483.25	FT	637.45	82	0.287	0.116	0.175
GR-1	SAFA-U	14370.08	15009.84	FT	639.764	149.2	0.246	0.067	0.531
GR-1	SAFA-L	15091.86	16359.5	FT	1267.64	420.8	0.236	0.053	0.479
KA-1	SAFA-U	13943.57	14796.59	FT	853.019	306.5	0.197	0.054	0.425
KA-1	SAFA-L	14796.59	15823.26	FT	1026.67	342.5	0.276	0.071	0.252
OP-2	SAFA-U	13943.57	14599.74	FT	656.168	583.9	0.16	0.106	0.196
OP-2	SAFA-L	14763.78	15976.75	FT	1212.97	986.2	0.17	0.169	0.151

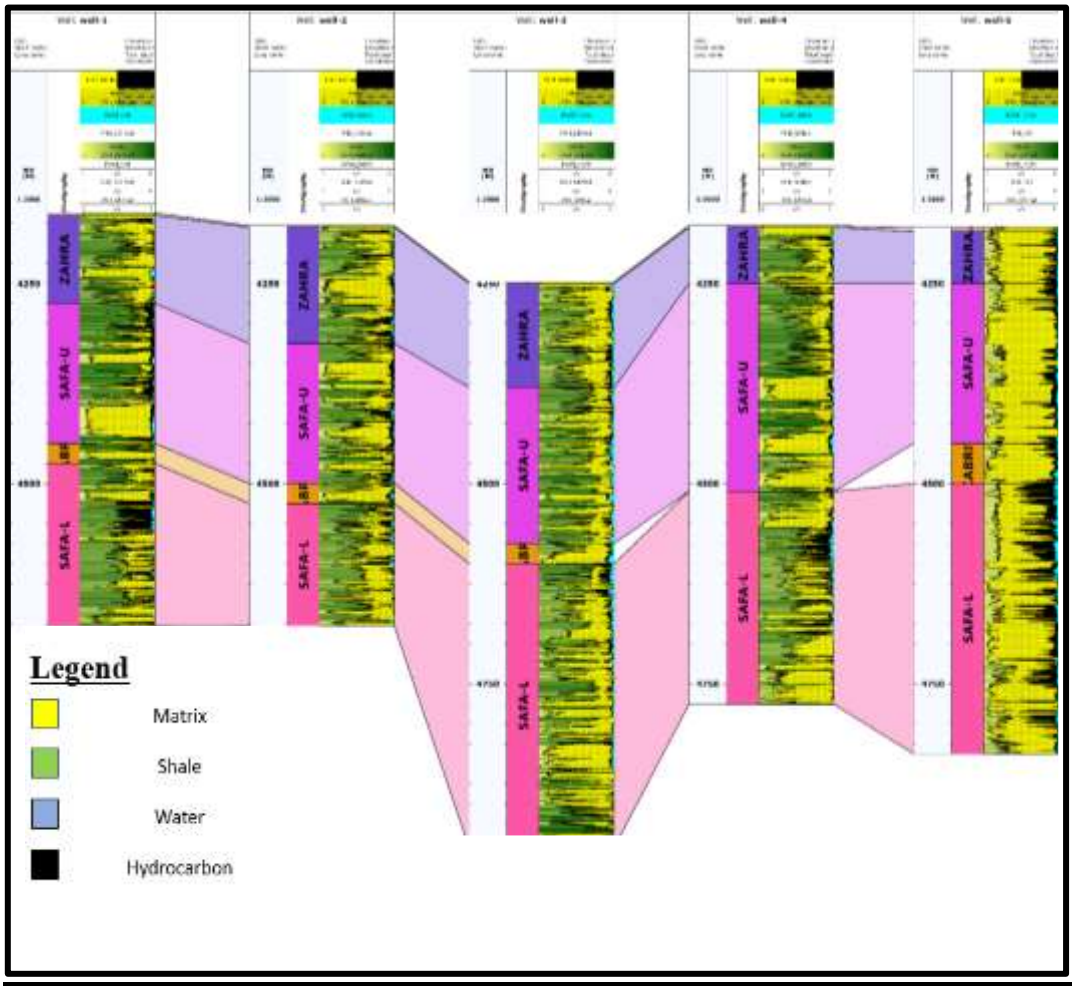

Figure 21: Well Correlation to L-Safa & U-Safa members across the wells.

6. Conclusions

Any well-log analyst could use this research sequence for any well-log data as it presents a full workflow to the petrophysical evaluation. This study found the following; Matruh-Shushan Basin offers a chance for hydrocarbon production through the Lower and Upper Safa Members. According to the petrophysical findings, the Five wells under investigation have hydrocarbon-bearing sand intervals, while these two members disappear at well-6. Mapping and area interpretation show that the reservoir's good quality increases to the N-E direction while shale volume decreases, effective porosity increases, and the water saturation decreases. So, well-5 is expected to produce the most among the six wells as it has more net to gross values and the best reservoir quality parameters.

7. Acknowledgements

The author would like to take this opportunity to thank everyone who has contributed to completing this paper. First and foremost, I would like to express my sincere gratitude to my supervisors for their invaluable guidance, feedback, and support throughout the research process. Their expertise, dedication, and encouragement have been crucial in shaping the direction of this work. I want to thank the participants, especially Mr Basem Chikiban, who generously gave their time and expertise to this study. Their willingness to share their experiences and insights was critical to the success of this research.

8. Conflict of Interest

The authors declare that they have no conflicts of interest.

References

[1] M. H. H. W. H. A. Mohamed Ragab Shalaby, "Geochemical characteristics and hydrocarbon generation modeling of the Jurassic source rocks in the Shoushan Basin, north Western Desert, Egypt," *Marine and Petroleum Geology,* vol. 28, no. 9, pp. 1611-1624, 2011.

[2] R. Said, The Geology of Egypt, California: Elsevier Publishing Company, 1962.

[3] G. Hantar, "North Western Desert," in *Geology of Egypt*, 1990, pp. 293-327.

[4] J. C. a. S. M. V. a. M. S. I. a. H. H. a. R. R. M. Dolson, "Egypt in the twenty-first century: petroleum potential in offshore trends," *GeoArabia,* vol. 6, no. 2, pp. 211--230, 2001.

[5] N. A. a. T. S. S. a. F. T. a. M. D. A. a. S. R. Ela, "Source rock evaluation of Kharita and Bahariya formations in some wells, North Western Desert, Egypt: visual palynofacies and organic geochemical approaches," *Egyptian journal of petroleum,* vol. 27, no. 4, pp. 455-465, 2018.

[6] R. Said, "The geology of Egypt," *Rotterdam, Brookfield,* vol. 734, 1990.

[7] Schlumberger, "Geology of Egypt," *Well Evaluation Conference,* pp. 1-64, 1984.

[8] EGPC, "Western desert, oil and gas fields, a comprehensive overview," *11th Petroleum Exploration and Production Conference, Egyptian General Petroleum Corporation,* p. 1–431, 1992.

[9] F. S. Millard, "Log Quality Control And Operational Efficiency Check," in *Fall Meeting of the Society of Petroleum Engineers of AIME,* New Orleans, Louisiana, 1963.

[10] Bigelow, "The "F" Overlay Technique and Construction of the M.O.P," 1972.

[11] D. G. J. S. a. J. D. Best, "A Computer-Processed Wellsite Log Computation," in *SPWLA 19th Annual Logging Symposium,* El Paso, Texas, 1978.

[12] W. Fertl, "Practical log analysis. Part 8. R/sub wa/method: fast formation evaluation," *Oil Gas J,* vol. 76, 1978.

[13] A. M. H. &. W. M. M. &. K. M. Farhoud, "Petrophysical analysis for Ammonite-1 well, Farafra Area, Western Desert, Egypt," *Arabian Journal of Geosciences,* vol. 7, no. 12, pp. 5107-5125, 2014.

[14] W. M. M. &. K. S. Soliman, "A numerical technique for an accurate determination of formation resistivity factor using FR-RO overlays method," *Arabian Journal of Geosciences,* vol. 8, no. 3, pp. 1291-1297, 2015.

[15] W. M. Mabrouk, "BVW as an indicator for hydrocarbon and reservoir homogeneity," *Journal of Petroleum Science and Engineering,* vol. 49, no. 1-2, pp. 57-62, 2005.

[16] G. Archie, "The Electrical Resistivity Log as an Aid in Determining Some Reservoir Characteristics," *Transactions of the AIME,* vol. 146, pp. 54-62, 1942.

[17] G. Pickett, "Pattern Recognition As A Means Of Formation Evaluation," in *SPWLA 14th Annual Logging Symposium,* Lafayette, Louisiana, 1973.

[18] W. M. M. A. I. M. Ahmed M. H. Metwally, "A numerical approach to accurately estimate water resistivity (Rw) and saturation (Sw) in shaly sand formations," *Contributions to Geophysics and Geodesy,* vol. 52, pp. 423-441, 2022.

[19] P. F. Worthington, "The Evolution Of Shaly-sand Concepts In Reservoir Evaluation," in *The Log Analyst 26,* 1985.

[20] R. Steiber, "Optimisation of shale volumes in open hole logs," *Journal of Petroleum Technology,* vol. 31, pp. 147-162, 1973.

[21] J. R. Hook, "An Introduction to Porosity," *Petrophysics-The SPWLA Journal of Formation Evaluation and Reservoir Description,* vol. 44, 2003.

[22] D. B. H. K.-C. P. M. A. A. M. D. B. N. R. T. L. K. J. A. W. J. R. Stephens, "A comparison of estimated and calculated effective porosity," *Hydrogeology Journal,* vol. 6, no. 1, pp. 156-165,

1998.

[23] Schlumberger Limited, Log Interpretation: Applications, Schlumberger, 1972.

[24] L. d. Witte, "Relations between resistivities and fluid contents of porous rocks," *Oil Gas J*, vol. 49, no. 16, pp. 120-134, 1950.

[25] P. Simandoux, "Dielectric measurements on porous media, application to the measurements of water saturation: study of behavior of argillaceous formations," *Revue de L'institut Francais du Petrole*, vol. 18, pp. 193-215, 1963.

[26] J. L. a. A. Poupon, "Evaluation Of Water Saturation In Shaly Formations," *The Log Analyst*, vol. 12, no. 4, 1971.

[27] A. Schlumberger, "A guide to well site interpretation of the gulf coast," Schlumberger Well Services, Houston, 1975., "A guide to well site interpretation of the gulf coast," *Schlumberger Well Services, Houston*, 1975.

[28] B. C. a. M. H. K. a. W. M. M. a. A. M. H. Metwally, "Petrophysical characterisation and formation evaluation of sandstone reservoir: Case study from Shahd field, Western Desert, Egypt," *Contributions to Geophysics and Geodesy*, vol. 52, pp. 443-466, 2022.

[29] M. &. M. W. &. M. A. &. B. A. &. E. S. Abuzaied, "Correlation of the reservoir characteristics from the well-logging data and core measurements in QASR field, north Western Desert, Egypt," *Arabian Journal of Geosciences*, vol. 13, 2020.

[30] M. B. A. Sarhan, "Seismic and well logging interpretation for evaluation of the lower Bahariya reservoir, southwest Qarun (SWQ) Field, Gindi Basin, Egypt," *Marine Geophysical Research*, vol. 38, 2017.